Coupled Plastic Wave Propagation and Column Buckling

Denzil G. Vaughn

James M. Canning

John W. Hutchinson

Division of Engineering and Applied Sciences,
Harvard University,
Cambridge, MA 02138

The plastic buckling of columns is explored in a regime where plastic wave propagation and lateral buckling are nonlinearly coupled. Underlying the work is the motivation to understand and quantify the dynamic crushing resistance of truss cores of all-metal sandwich plates where each truss member is a clamped column. Members are typically fairly stocky such that they buckle plastically and their load carrying capacity decreases gradually as they buckle, even at slow loading rates. In the range of elevated loading rates of interest here, the columns are significantly stabilized by lateral inertia, resisting lateral motion and delaying buckling and loss of load carrying capacity to relatively large overall plastic strains. The time scale associated with dynamic axial behavior, wherein deformation spreads along the column as a plastic wave, is comparable to the time scale associated with lateral buckling such that the two phenomena are coupled. Several relevant problems are analyzed using a combination of analytical and numerical procedures. Material strain-rate dependence is also taken into account. Detailed finite element analyses are performed for axially loaded columns with initial imperfections, as well as for inclined columns in a truss core of a sandwich plate, with the aim of determining the resistance of the column to deformation as dependent on the loading rate and the relevant material and geometric parameters. In the range of loading rates of interest, dynamic effects result in substantial increases in the reaction forces exerted by core members on the faces of the sandwich plate with significant elevation in energy absorption.
[DOI: 10.1115/1.1825437]

1 Introduction

Pursued extensively for over 50 years, the dynamic axial loading of columns is still an important subject because of its relevance to a wide range of engineering applications. Much interesting mechanics underlies qualitative and quantitative understanding of dynamic column buckling, and the subject has not been without controversy. Here, columnar truss members of all metal truss core sandwich plates motivate the study as these sandwich plates have the potential for replacing solid plate construction for a range of applications including ship hulls, armored vehicles, and chemical plants [1] where impulsive loads are of concern. For applications involving high intensity dynamic crushing loads, cores can experience nominal strain rates greater than $10^3\ s^{-1}$. Column members in truss cores are usually sufficiently stocky such that buckling occurs well into the plastic range, especially when the columns are stabilized by lateral inertia at elevated loading rates. The basic cellular unit of a tetragonal truss core is shown in Fig. 1. Although the columns in the core are inclined with respect to the crushing direction, they nevertheless behave in a manner similar to an axially compressed column due to the fact that their end displacements are constrained by the face sheets in the direction parallel to the sheets. Of primary interest is the resistance of the columns to deformation, the forces they exert on the face sheets during dynamic crushing, and the energy they absorb. Most of the emphasis in this paper will be on axially compressed columns, but the direct relevance of results for axially compressed columns to inclined columns will be demonstrated in the second half of the paper.

There is a large literature on dynamic plastic buckling of columns [2–5] and perhaps a rationale for further study is warranted. In the applications motivating this study, a representative column would be relatively stocky, typically 0.1 m in length, and subject to a suddenly imposed velocity on the order of $100\ ms^{-1}$ at one end corresponding to an overall strain rate of $10^3\ s^{-1}$. The loading rates of interest are such that the initial stages of the deformation are dominated by the propagation of a plastic axial wave down the column. Buckling is resisted by lateral inertia. Overall compressive strains of 20% or more can be achieved before appreciable buckling deflections occur. Buckling deflections, which depend on initial imperfection amplitudes, develop in the later stages of the crushing. Thus, during the initial stage of deformation, the forces exerted on the face sheets are similar to those exerted by a straight rod undergoing dynamic axial deformation. As buckling deformations develop, the forces depend in a complicated way on coupled plastic wave propagation and lateral buckling.

The early study of Abrahamson and Goodier [3] on column impact has aspects in common with the problem and loading rates of interest here. Specifically, their experiments involved impact velocities in the range of interest here, and overall compressive strains on the order of 20% due primarily to axial straining were observed. However, the primary motivation underlying the work in [3] was buckling and not the forces exerted during the impact. In addition, the theoretical approach of these authors was to decouple the axial deformation from the buckling deformation by assuming the axial stress state was established prior to the growth of buckling deformations. Calladine and English [5] also decoupled axial deformations from bucking deformations in their study of the various influences of inertia on dynamic buckling. As will be seen in the body of the paper, this decoupling is justified since their work focused on a range of relatively low impact velocities; the maximum impact velocity in their experiments did not exceed $10\ ms^{-1}$. These authors make the important observation that inertial stabilization effects scale differently with column size than material strain-rate effects, a point that will be discussed in the present paper as well.

The problem that couples plastic wave propagation and lateral buckling has only recently received attention [6–8], with analyti-

Contributed by the Applied Mechanics Division of THE AMERICAN SOCIETY OF MECHANICAL ENGINEERS for publication in the ASME JOURNAL OF APPLIED MECHANICS. Manuscript received by the Applied Mechanics Division, April 21, 2004; final revision, May 3, 2004. Editor: R. M. McMeeking. Discussion on the paper should be addressed to the Editor, Professor Robert M. McMeeking, Journal of Applied Mechanics, Department of Mechanical and Environmental Engineering, University of California-Santa Barbara, Santa Barbara, CA 93106-5070, and will be accepted until four months after final publication in the paper itself in the ASME JOURNAL OF APPLIED MECHANICS.

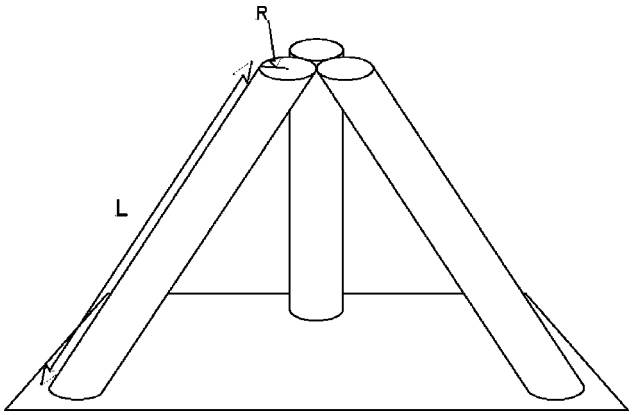

Fig. 1 Tetragonal Truss Core

cal and numerical approaches with primary emphasis on the buckle shape. Here, the coupled nonlinear problem is analyzed using a numerical approach, accounting for both imperfections and material strain rate dependence, with emphasis on the forces required to deform the column and the energy dissipated by the column. However, to shed light on the initial stages of the deformation history, the next section of the paper presents results for the propagation of plastic axial waves down a rod following the classic treatments of von Karman and Duwez [9] and Taylor [10]. An important dimensionless loading rate parameter tied to the dynamic effects emerges from this analysis. The fully coupled problem is analyzed for a wide range of loading rates utilizing the commercially available codes ABAQUS/Standard and ABAQUS/Explicit. Reaction forces and energy dissipation are determined as a function of geometric, material and loading parameters. With the aid of numerical analysis, it is also demonstrated that the forces exerted on the face sheets by inclined columns in a truss core can be well approximated using results for the axially compressed column.

2 Uniaxial Waves in a Rod

2.1 Wave Equation for Rate-Independent Material. Taylor [10] and von Karman and Duwez [9] considered a one-dimensional plastic wave propagating down a rod. Taylor's approach was conducted within a finite strain setting, and a similar approach will be followed here, but with a different choice of variables. (Several authors have remarked to the effect that von Karman and Duwez also use a finite strain approach in their analysis, but their treatment of finite strain aspects is not nearly as transparent as that of Taylor.) Consider a semi-infinite bar extending from $x=0$ to $x=\infty$ at $t=0$, with a material point at x at $t=0$ located at $X=x+u(x,t)$ at t. The logarithmic (true) strain is related to the displacement gradient by $\varepsilon=\ln(1+\partial u/\partial x)$. Analytical solutions are restricted to rods made of rate-independent materials such that the true stress (force per current area) can be regarded as a function of true strain, $\sigma(\varepsilon)$. Material rate-dependence is taken into account in Sec. 2.3. In this subsection and the next, attention is limited to problems with monotonic straining such as a compression wave with no elastic unloading. Following the earlier work of Taylor and von Karman and Duwez, the rod is assumed to be incompressible and the effect of radial inertia is neglected. With A as the cross-sectional area of the rod in the deformed state and $F=\sigma A$ as the force carried by the rod, equilibrium requires $\partial F/\partial X=\rho A\partial^2 u/\partial t^2$, where ρ is the density of the material. Incompressibility implies $dA/d\varepsilon=-A$. When expressed in terms of $u(x,t)$, the equilibrium equation can be written as

$$\frac{\partial^2 u}{\partial x^2}=\frac{1}{c(\varepsilon)^2}\frac{\partial^2 u}{\partial t^2} \tag{1}$$

where the strain-dependent wave speed is

$$c(\varepsilon)=\sqrt{\frac{E_t-\sigma}{\rho}}e^{-\varepsilon} \tag{2}$$

and $E_t=d\sigma/d\varepsilon$ is the tangent modulus of the true stress-log strain curve. The wave speed, E_t, σ, and ε all depend on u through the expressions listed above.

Three limiting cases of (1) and (2) are worth identifying. When yielding occurs with small strains and $E_t\gg|\sigma|$, $c=\sqrt{E_t/\rho}$, which is often referred to as the plastic wave speed. The finite strain formulation gives $c=\sqrt{\sigma_Y/\rho}$ for a plastic compression wave propagating along an elastic-perfectly plastic rod ($E_t=0$) where σ_Y is the yield stress. The wave speed of a tensile wave approaches zero when $\sigma=E_t$, corresponding to the Considere condition for necking localization.

2.2 Compression Wave in an Infinitely Long Bar Subject to Constant Velocity at Its End. The solution produced independently during World War II by von Karman and Duwez [9] and Taylor [10] for uniaxial impact loading of a long rod provides insight to the column problems of interest in this paper. Specifically, at the higher rates of loading of interest, the column remains nearly straight in the early stage of deformation and behavior is dominated by an axial plastic compression wave.

For the case of a semi-infinitely long bar ($0\leqslant x<\infty$) at rest at $t=0$ and subject to a uniform velocity, $\dot{u}(0,t)=V>0$, at its left end, a similarity solution to (2) exists [9,10] with dependence on a single dimensionless variable $\xi=x/(c_0 t)$ where $c_0=c(0)=\sqrt{E/\rho}$ is the elastic wave speed with E as Young's modulus. The solution is simple but highly nonlinear and implicit. Only the details of interest will be presented here. The solution depends on the relation between ε and ξ defined by $c(\varepsilon)/c_0=\xi$ and the inverse of this relation denoted by $\varepsilon=g(\xi)$. The regime $\xi>1$ lies ahead of the disturbance; the regime $\xi_U<\xi<1$ has the strain dependence $\varepsilon=g(\xi)$; and the regime $0<\xi<\xi_U$ has uniform strain with $\varepsilon\equiv\varepsilon_U=g(\xi_U)$ and uniform velocity $\dot{u}=V$. The front of the section of the rod having uniform strain ε_U and velocity V propagates down the rod with speed $c(\varepsilon_U)$. The transition value ξ_U depends on the imposed velocity V according to the highly implicit equation

$$(1-e^{g(\xi_U)})\xi_U+\int_{\xi_U}^{1}(1-e^{g(\xi)})d\xi=\frac{V}{c_0} \tag{3}$$

The solution is illustrated for a Ramberg–Osgood stress–strain relation

$$\frac{\varepsilon}{\varepsilon_Y}=\frac{\sigma}{\sigma_Y}+\left(\frac{\sigma}{\sigma_Y}\right)^n \tag{4}$$

with yield stress σ_Y, yield strain $\varepsilon_Y=\sigma_Y/E$, strain hardening exponent $N=1/n$ $(0<N<1)$ and tangent modulus

$$\frac{E}{E_t}=1+n\left(\frac{\sigma}{\sigma_Y}\right)^{n-1} \tag{5}$$

Details of the solution, which must be obtained numerically using (3), are plotted in Fig. 2. Both the strain and the nominal compressive stress (compressive force per original area, $\sigma_N=-\sigma e^{-\varepsilon}$) in the uniformly strained region are displayed.

An analytical approximation is obtained by assuming the strains are small and neglecting σ compared to E_t in (2) such that $c(\varepsilon)=\sqrt{E_t/\rho}$. Then, neglecting the linear stress contribution to the strain in (4), it is readily shown that $g(\xi)=-\varepsilon_Y(\xi/\sqrt{N})^{-2/(1-N)}$ with

$$\frac{\varepsilon_U}{\varepsilon_Y}=-\left[\frac{1+N}{2\sqrt{N}}\left(\frac{V}{c_0\varepsilon_Y}\right)\right]^{2/(N+1)} \tag{6}$$

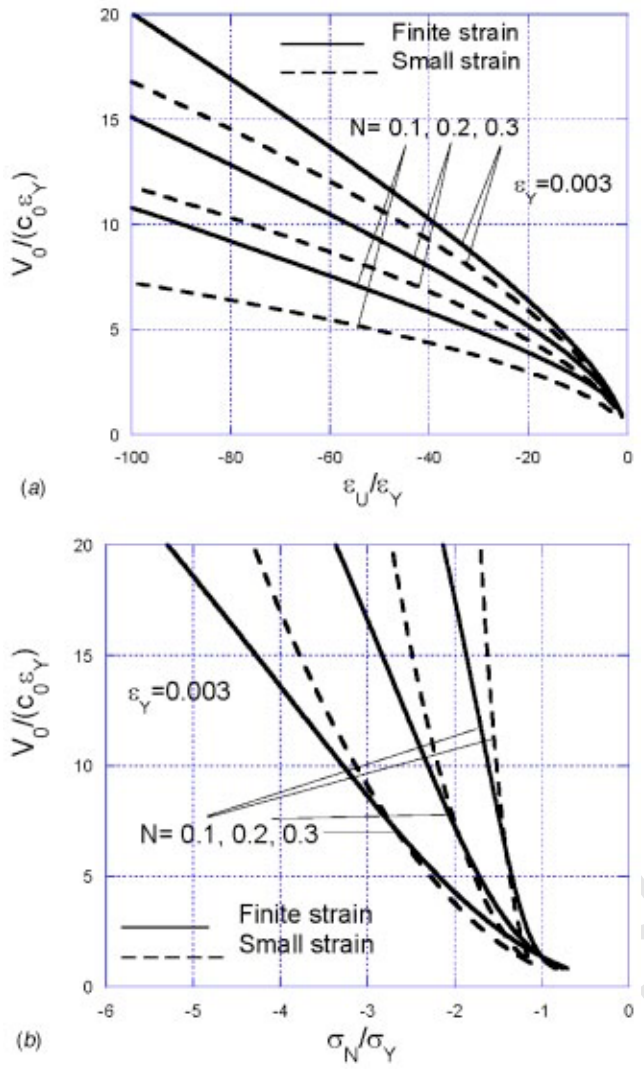

Fig. 2 Plastic compression wave propagating along a rod for both the small strain approximation and the finite strain solution. (*a*) Strain ε_U in the region of uniform deformation behind the propagating front. (*b*) Nominal compressive stress at the left end of the rod and in the adjacent region of uniform strain. The normalizations for the small strain approximation are valid for all yield strains; the results for the finite strain solution are computed with $\varepsilon_Y = 0.003$.

$$\frac{\sigma_N}{\sigma_Y} = \left[\frac{1+N}{2\sqrt{N}}\left(\frac{V}{c_0\varepsilon_Y}\right)\right]^{2N/(N+1)} \tag{7}$$

$$\frac{c(\varepsilon_U)}{c_0} = \sqrt{N}\left[\frac{1+N}{2\sqrt{N}}\left(\frac{V}{c_0\varepsilon_Y}\right)\right]^{-(1-N)/(1+N)} \tag{8}$$

The small strain solution depends on the imposed velocity, V, and initial yield strain through the single parameter, $V/c_0\varepsilon_Y$, which will be seen to be the most important dimensionless parameter governing dynamic effects in the present study. The small strain approximation is also plotted in Fig. 2, where it is seen that it is indeed captures the essential trends for $V/c_0\varepsilon_Y$ as large as about 20. The front of the uniformly strained section of the rod propagates at a small fraction of the elastic wave speed when $V/c_0\varepsilon_Y \approx 10$, corresponding to imposed velocities V that are typically several percent of the elastic wave speed. Since an initial yield strain usually lies within the range from 0.001 to 0.01, it follows

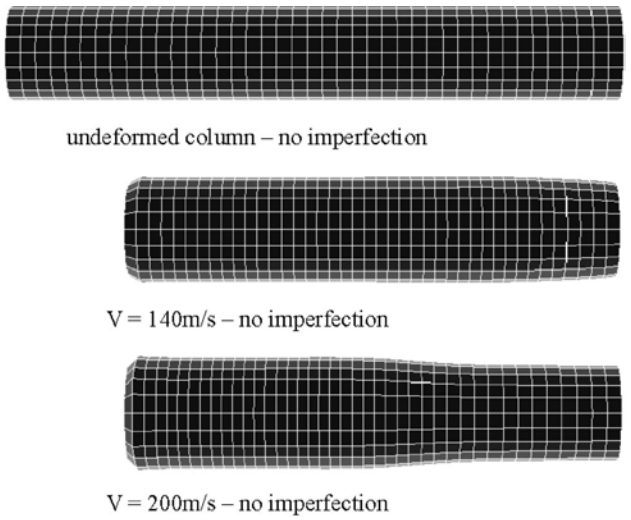

Fig. 3 Undeformed and deformed meshes for a rod subject to velocities $V = 140$ ms^{-1} and $V = 200$ ms^{-1} [$V/(c_0\varepsilon_Y) = 13.3$ and 19] at its left end and fixed at its right end. The deformed rods have been deformed to an overall strain of 20%. No material rate dependence.

that for structural metals plastic wave propagation effects become dominantly important for impact velocities V typically in the range from 10 to 100 ms^{-1}.

2.3 Dynamic Compression of Finite Length Rods. In this section the study of dynamic compressive behavior of the straight column, or rod, is continued accounting the effect of finite length. As in the previous section, the rod is initially at rest. At $t = 0$, a uniform velocity, $V > 0$, is imposed at its left end while the right end at $x = L$ is fixed. In the study in this subsection the material is taken to be the rate-independent limit of a structural stainless steel, Al6XN, currently being considered as a possible candidate for truss cores. This material has substantial strain hardening that is nearly linear and moderate strain-rate sensitivity. The full rate-dependent specification of the material is given below in anticipation of its use in subsequent sections. In tension, the relation between true stress and true strain is taken to be strictly bilinear for each value of plastic strain-rate:

$$\sigma = \begin{cases} E\varepsilon, & \varepsilon \leqslant \varepsilon_Y(1+(\dot{\varepsilon}_p/\dot{\varepsilon}_0)^m) \\ \sigma_Y(1+(\dot{\varepsilon}_p/\dot{\varepsilon}_0)^m) + E_t\varepsilon_p, & \varepsilon > \varepsilon_Y(1+(\dot{\varepsilon}_p/\dot{\varepsilon}_0)^m) \end{cases} \tag{9}$$

with $E = 190$ GPa, $\sigma_Y = 400$ MPa, $E_t = 2.4$ GPa, $\dot{\varepsilon}_0 = 4920$ s^{-1}, $m = 0.154$, $\rho = 7920$ kg m^{-3}, and Poisson's ratio $\nu = 0.3$. The strain-rate dependence results in a 57% elevation of the stress for $\dot{\varepsilon} = 1000$ s^{-1} versus the stress at $\dot{\varepsilon} = 0.01$ s^{-1} at the same ε_p. The rate-independent limit used in this section is obtained by setting $m = 0$. Comparisons will be made between predictions with and without rate-sensitivity in the following sections.

The finite strain version of ABAQUS Explicit [11] has been used to compute the responses. The right face of the column is attached to a fixed rigid plate and left face of the column is attached to a rigid plate with prescribed uniform velocity V for $t \geqslant 0$. The column model is comprised of eight-noded linear hexahedral elements. The model accounts for radial inertia. In the computations, the initial length of the rod is $L = 0.122$ m and its radius R is taken to be $L/13$. An undeformed mesh and a representative deformed mesh at an overall compressive strain of 20% are shown in Fig. 3 for two values of V Further mesh refinement does not appreciably alter the results discussed below. The range of imposed velocities of relevance to the applications described in the Introduction is $V/(c_0\varepsilon_Y) \leqslant 20$.

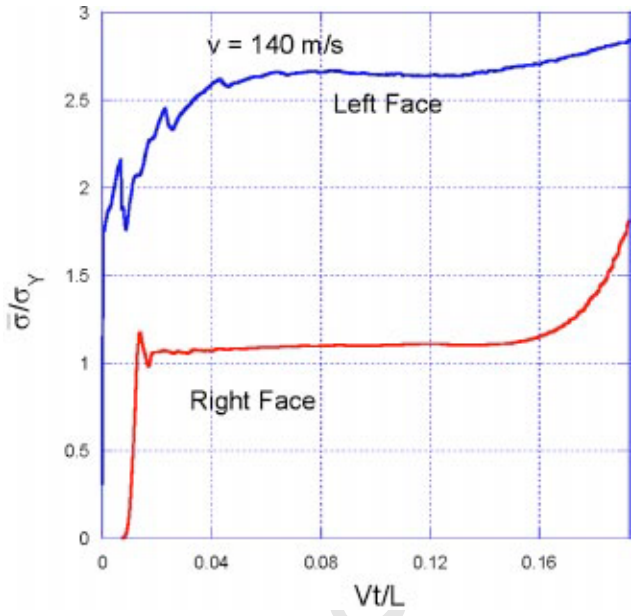

Fig. 4 Nominal stress exerted by a rod on the plates at its two ends, where the left plate impacts the rod at $V=140$ ms^{-1} $[V/(c_0\varepsilon_Y)=13.3]$ and the right plate is fixed.

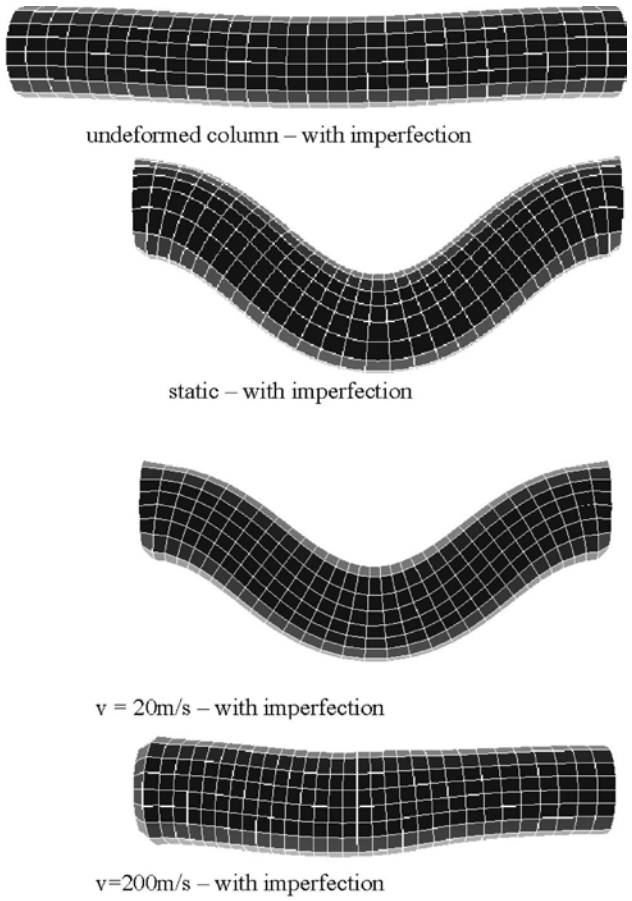

Fig. 5 Undeformed and deformed meshes of column with initial imperfection for quasistatic, $V=20$ m/s, and $V=200$ m/s $[V/(c_0\varepsilon_Y)=1.9]$ and high $[V/(c_0\varepsilon_Y)=19]$. No material rate dependence.

The response of the column to a constant velocity $V=140$ m/s $[V/(c_0\varepsilon_Y)=13.3]$ is shown in Fig. 4. The forces on the left and right plates are shown. Oscillations in the force on the left plate at early times in the history are due to numerical effects associated with the abrupt increase of the applied velocity. To reduce these oscillations, the applied velocity on the left plate is increased from zero to V in a more gradual manner according to $V(1-e^{-t/t_0})$. The oscillations are largely smoothed out and behavior for $Vt/L>0.05$ is virtually unaffected by the choice of t_0 as long as $V_0 t_0/L<0.02$. Oscillatory effects are much smaller on the right face since there is no response until the arrival of the compression wave.

Aside from oscillations at early times, the force on the left plate is fairly constant throughout the deformation and well above with the yield stress, consistent with the results for the infinitely long rod discussed in the previous section. The force on the left face remains level to a nominal overall strain of 20% ($Vt/L=0.2$), at which point the computation was terminated. Thus, due to inertial effects there is a significant difference between the force a core element will exert on the face sheet towards a blast loading and on the face sheet away from the blast. The deformed mesh in Fig. 3 shows the rod at 20% strain ($Vt/L=0.2$) where the thicker, uniformly compressed region has just reached the far end in the case $V=140$ m/s, while for the rod subject to the higher end velocity $V=200$ m/s the compressed region has only spread over two-thirds the length of the rod at the same overall strain.

Results such as those shown in Fig. 4 have been computed for 20 m/s$\leqslant V\leqslant$200 m/s. For $V<20$ m/s $[V/(c_0\varepsilon_Y)<1.9]$, dynamic effects are not nearly so pronounced with plastic deformation occurring more uniformly along the rod and end forces that are nearly equal.

3 Coupled Plastic Wave Propagation and Lateral Buckling for Axially Compressed Columns

In this section, results for the straight, finite length column analyzed in the previous section are determined under circumstances where the column is permitted to buckle. The material comprising the column is described by (9) which includes rate-dependence, however, results will be presented to highlight the roles of both strain hardening and strain-rate dependence. As in the study of the previous section, the ends of the column are ''welded'' to rigid plates and thus effectively clamped against rotation at each end. The left plate experiences an imposed uniform velocity V starting at $t=0$, while the right end is fixed. The dynamic calculations are carried out using a three-dimensional meshing using hexahedral elements with ABAQUS Explicit; quasi-static calculations use the Standard version. A geometric imperfection is introduced to promote lateral buckling motion in the form of an initial transverse deflection

$$w(x)=\frac{\zeta R}{2}\left[1-\cos\left(\frac{2\pi x}{L}\right)\right] \tag{10}$$

where ζ is the normalized imperfection amplitude. As will be shown later, an axially compressed column with imperfection amplitude $\zeta=1/4$ provides a reasonable approximation to the response of the tetragonal truss core construction where the members are inclined but have no initial imperfection. Under dynamic conditions, a perfectly straight column that is not inclined does not buckle, assuming no other imperfections due either to loading or material asymmetry. The nature of the governing equations is such that solution bifurcations do not occur. Dynamic buckling requires an initial asymmetric imperfection of some type, and, moreover, the development of the lateral buckling motion depends on the imperfection amplitude. For relatively stocky columns of interest here, an imperfection with $\zeta=1/4$ can be regarded as realistic, and later it will be shown that the buckling response is not a strong function of ζ in this range.

The role of inertia in altering the column response is illustrated in Fig. 5 where deformed columns at a nominal strain of 20% are

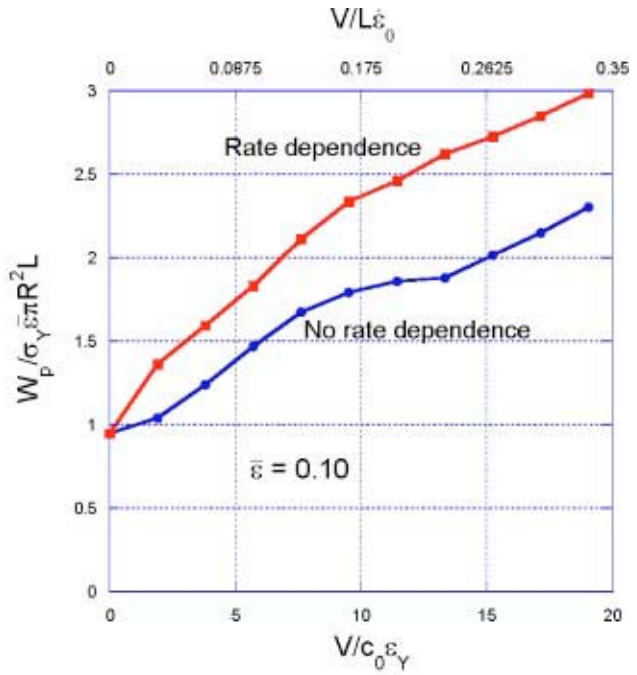

Fig. 6 Plastic energy dissipation as a function of $V/(c_0\varepsilon_Y)$ [and $V/(L\dot{\varepsilon}_0)$], with and without strain-rate dependence at an overall strain $\bar{\varepsilon}=0.1$ for the material specified by (9) and $c_0\varepsilon_Y/(L\dot{\varepsilon}_0)=0.0175$.

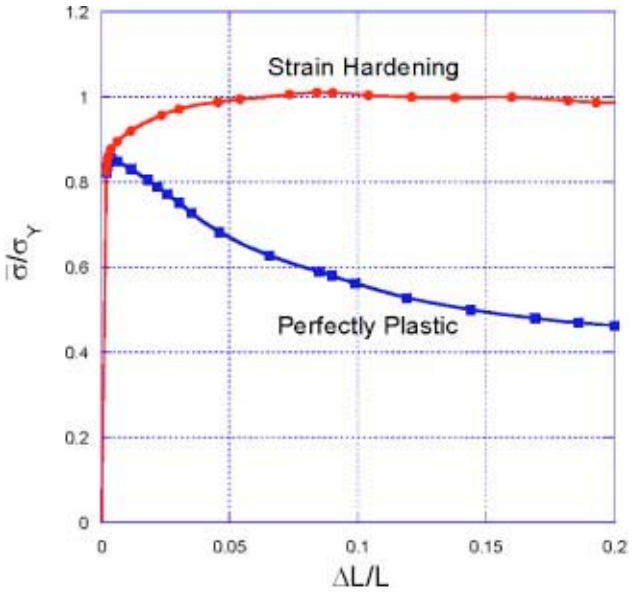

Fig. 7 Quasistatic nominal stress-end shortening behavior with and without strain hardening. The material is specified by (9) with $E_t=0$ and $m=0$ for the elastic-perfectly plastic case and $E_t=2.4$ GPa and $m=0$ for the hardening material. The stockiness ratio is $R/L=0.077$ and the imperfection amplitude is $\zeta=1/4$.

shown for very slow (quasistatic loading) and two other imposed velocities, $V=20$ m/s and 200 m/s. The buckled shapes of the quasistatically loaded column and that with $V=20$ m/s are similar and representative of the classical mode of a clamped beam. By contrast, the column loaded with $V=200$ m/s ($V/\varepsilon_Y c_0=19.4$) has undergone relatively little lateral displacement even at an overall strain of 20% and it is evident from the deformed shape that the majority of compression has occurred within the left half of the column. The plastic wave traveling from the left end has not yet spread over the entire column at the instant of the deformation in Fig. 5, and lateral buckling is just beginning to develop.

There are important consequences of the dynamic stabilization of the columns against lateral buckling seen in Fig. 5. In applications of all-metal sandwich construction for blast resistant plate structures, energy absorption in the core is an important component of superior performance. Any delay of buckling of a truss core member due to inertial stabilization translates into greater plastic energy dissipation. The column in Fig. 5 loaded at $V=200$ m/s has absorbed the energy equivalent of the material strained to 20% under uniaxial compression, albeit nonuniformly along its length. The energy absorbed by the column loaded quasistatically to 20% overall strain is considerably less since it undergoes significant lateral buckling and loss of load carrying capacity. Under uniaxial compression, energy absorption scales with $\sigma_Y\bar{\varepsilon}\pi R^2L$, where $\bar{\varepsilon}=Vt/L$ is the overall strain, and Fig. 6 displays the plastic energy dissipation in the column at $\bar{\varepsilon}=0.1$ normalized by this factor as a function of $V/(\varepsilon_Y c_0)$, with and without material strain-rate dependence. This plot brings out the exceptionally strong influence of dynamic loading on plastic dissipation as measured by the parameter $V/(\varepsilon_Y c_0)$; energy absorption can be enhanced by a factor of 2 or more in the range $V/(\varepsilon_Y c_0)>10$.

AL6XN has moderately high strain hardening. To separate out the influence of strain hardening on inertial stabilization and its related effects, columns of elastic-perfectly plastic material are investigated with the same initial yield stress as AL6XN in (9). The overall load-end shortening responses under quasistatic loading with and without strain hardening (both materials have $m=0$) are plotted in Fig. 7, where each of the two columns have an initial imperfection with $\zeta=1/4$. High strain hardening leads to significantly more postbuckling load carrying capacity. The substantial quasistatic postbuckling capacity for both columns is a consequence of their relative stockiness ($L/R=13$) and the fact that they are clamped on both ends.

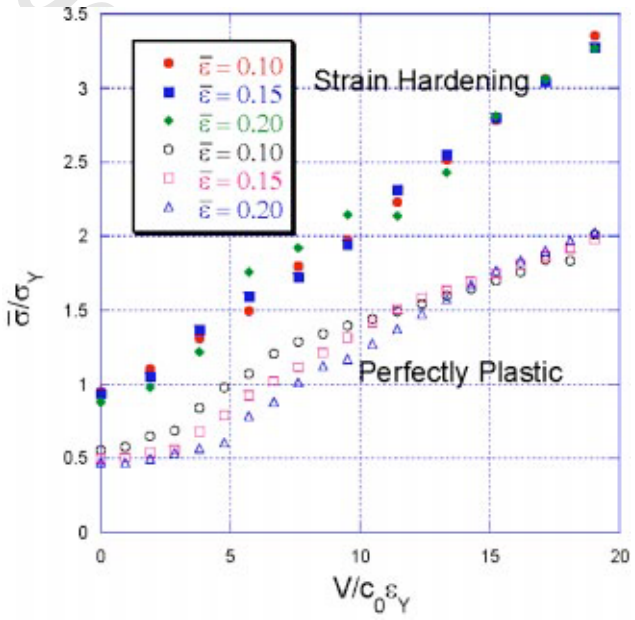

Fig. 8 Nominal stress acting by the column on the left plate as a function of the normalized imposed velocity V at three levels of overall strain for both an elastic-perfectly plastic material [(9) with $E_t=0$ and $m=0$] and a material with high strain hardening [(9) with $E_t=2.4$ GPa, $m=0$]. The imperfection amplitude is $\zeta=1/4$.

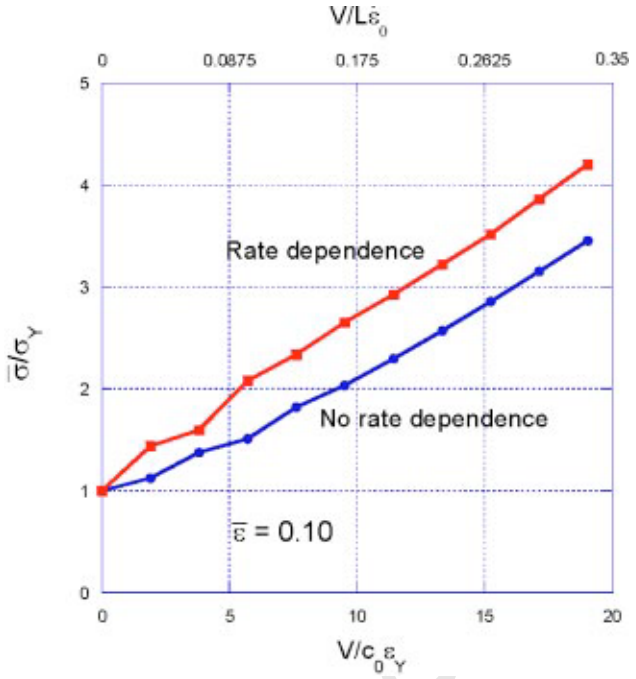

Fig. 9 Nominal stress acting by the column on the left plate as a function of the normalized imposed velocity V for a strain hardening material (9) with ($m=0.154$) and without ($m=0$) strain-rate dependence at an overall strain of 10%. The imperfection amplitude is $\zeta=1/4$ and $c_0\varepsilon_Y/(L\dot{\varepsilon}_0)=0.0175$.

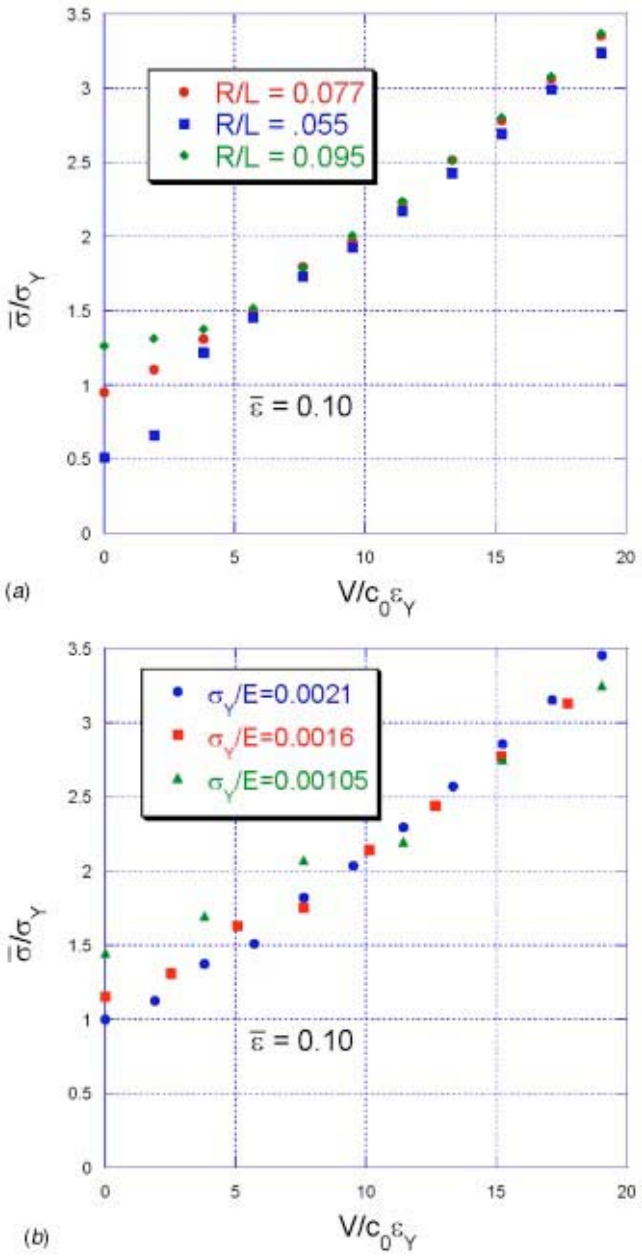

Fig. 10 (*a*) Effect of the stockiness, R/L, on the nominal stress acting by the column on the left plate as a function of the normalized imposed velocity V for a strain hardening material with no strain-rate dependence [(9) with $E_t=2.4$ GPa, $m=0$]. The imperfection amplitude is $\zeta=1/4$. (*b*) Effect of the yield strain, $\varepsilon_Y=\sigma_Y/E$, on the nominal stress acting by the column on the left plate as a function of the normalized imposed velocity V for a strain hardening material with no strain-rate dependence [(9) with $E_t=2.4$ GPa, $m=0$]. The imperfection amplitude is $\zeta=1/4$.

Computed values of the normalized force exerted by the column on the plate on the left end as a function of imposed velocity are given in Fig. 8 for a column of elastic-perfectly plastic material and of strain hardening typical of AL6XN in (9), both with no rate-dependence ($m=0$). With F as the force, the normalization is $\overline{\sigma}/\sigma_Y$, where $\overline{\sigma}=F/A_0$ is the nominal stress and A_0 is the initial cross-sectional area of the column. It can be seen that the force is nearly independent of strain, consistent with the responses discussed earlier in Fig. 4, except for the elastic-perfectly plastic column at low levels of imposed velocity. The most striking feature of the results in Fig. 8 is the large amplification of the force exerted by the column on the left plate as V is increased. Force amplification arises from two sources: (1) inertial stabilization of the column against buckling and (2) the momentum imparted to the column by the left plate. The component associated with inertial stabilization gives rise to the increased plastic dissipation of Fig. 6.

The effect of material strain-rate dependence on the reaction force on the left plate is shown in Fig. 9. The lower curve is that discussed for AL6XN with strain-rate dependence suppressed [$m=0$ in (9)] while the upper curve incorporates the strain-rate dependence of this material. When material rate-dependence is taken into account, additional dimensionless parameters arise: m and $V/(L\dot{\varepsilon}_0)$. The results in Fig. 9 include the values of $V/(L\dot{\varepsilon}_0)$ on the abscissa. The elevation of the reaction force due to material strain-rate dependence over the corresponding force for the rate-dependent material is what would be expected for the overall strain rate of 10^3 s^{-1} [corresponding to the impact velocity with $V/(\varepsilon_Y c_0)=11.6$ in Fig. 9]; the influence is similar to that seen in Fig. 6 on the energy dissipation.

Based on dimensional considerations, the normalized reaction force depends on a relatively large dimensionless parameter set according to

$$\frac{\overline{\sigma}}{\sigma_Y}=f\left(\frac{V}{\varepsilon_Y c_0},N,\frac{\sigma_Y}{E},\frac{R}{L},\frac{Vt}{L},\frac{V}{L\dot{\varepsilon}_0},m\right) \tag{11}$$

with $c_0=\sqrt{E/\rho}$. Equation (11) brings out the point emphasized by Calladine and English [5] that inertial effects and material rate-dependence effects scale differently with respect to column length. In the range of behavior in which inertial effects are dominated by axial deformation, the controlling parameter is $V/(\varepsilon_Y c_0)$. The dimensionless parameter controlling the influence of material rate-dependence is $V/L\dot{\varepsilon}_0$. The results presented above suggest that the dependence of end forces and energy dissipation on material strain-rate dependence through m and $V/L\dot{\varepsilon}_0$ is more-or-less what would be expected at the overall strain-rate,

given its effect in elevating the flow stress in (9). In the range of overall strain Vt/L from 0.05 to more than 0.2, the normalized reaction force is essentially independent of strain for relatively stocky columns, except for small strain hardening at low imposed velocities.

The effect of the slenderness ratio, R/L, and the initial yield strain, $\varepsilon_Y = \sigma_Y/E$, on the normalized reaction force at an overall strain of 10% are shown in Figs. 10(*a*), 10(*b*). The slenderness ratio has a significant effect at small $V/(\varepsilon_Y c_0)$ but almost no effect at higher values of this parameter, consistent with the fact that the buckling deflections remain small until overall strains in excess of 20%. Similarly, for the normalizations used in Fig. 10(*b*), there is little dependence on the initial yield strain.

In summary, for a specific material in the range of imposed velocities satisfying $V/(\varepsilon_Y c_0) > 5$ and for overall strains from roughly 5% to 20%, the single most important dimensionless parameter in (11) is $V/(\varepsilon_Y c_0)$, with $V/L\dot{\varepsilon}_0$ playing a secondary role, such that the nominal reaction stress resisting the motion of the plate imposing its velocity on the column has the form

$$\frac{\bar{\sigma}}{\sigma_y} = f\left(\frac{V}{\varepsilon_Y c_0}, \frac{V}{L\dot{\varepsilon}_0}\right). \tag{12}$$

4 The Dynamic Response of Tetragonal Truss Core

Finite element calculations have been performed on the tetragonal truss core unit of Fig. 1 under conditions where the rigid bottom plate is held fixed and the rigid top plate to which the core faces are welded is suddenly accelerated towards the bottom plate with velocity V. The emphasis here is on the reaction force exerted by the core element on the top plate, and it will be shown that this resistance can be successfully modeled using the results for the axially loaded columns of the previous section. Each member of the unit of the regular tetrahedron in Fig. 1 is a column of length L and solid circular cross-section of radius R with $R/L = 0.077$. The precise geometry is shown in Fig. 1. The height, H of the core is specified by $H/L = \sqrt{2/3}$. The material is that specified in (9) with no strain rate dependence ($m = 0$). Results are computed for various imposed velocities for overall strains up to 20% ($\bar{\varepsilon} = Vt/H = 0.2$). The average reaction stress, $\bar{\sigma}$, acting on the top plate and plotted in Fig. 11 is the net vertical force divided by the area of the tetragonal unit. The results of the simulations for the tetragonal core are plotted as solid points. As in the case of the axially loaded columns, there is relatively weak dependence on overall strain for strains in the range from 5% to 20%.

The insert in Fig. 11 compares the deformed shape of a member of the tetragonal unit for a case with quasistatic loading with one subject to high velocity loading, both at an overall strain of about 20%. The deformation of the dynamically loaded member is primarily confined to its upper third while the lower portion of the member remains almost straight. By contrast, the member deformed quasistatically undergoes bending deformations due to buckling over its entire length.

Included in Fig. 11 are predictions of the average reaction stress based on the results obtained in the previous section for the axially loaded clamped column with three levels of initial imperfection. To plot the results based on the axially loaded column, the length and aspect ratio of the column are identified with those of the inclined member. Furthermore, the axial velocity applied to the upper end of the column is the component of the approach velocity of the two plates resolved in the direction parallel to the column, i.e. $\sqrt{2/3}V$, and, as before, the lower end is fixed. Similarly, the vertical component of the reaction force acting on the upper plate is taken to be $3\sqrt{2/3}$ times the axial force in the column and converted to the stress averaged over the unit cell in Fig. 11. Since the results for the axial column are almost independent of the overall strain in the range from 5% to 20% (cf. Fig. 8), only the average over the strain range is plotted in Fig. 11 for the column approximation. The effect of the initial imperfection level is not large for the three levels shown and $\zeta = 1/4$ seems to be a realistic choice. Finally, it is noted that the results based on those for the axially compressed column provide a reasonable approximation to the reaction force exerted by the tetragonal core.

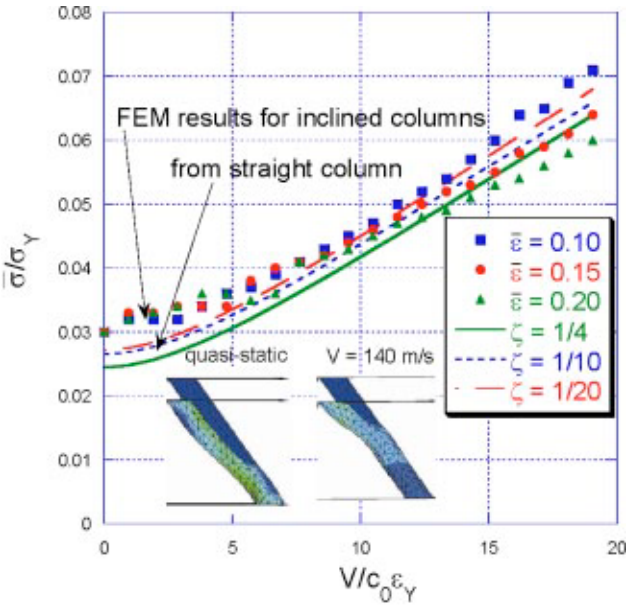

Fig. 11 Normal component of reaction force exerted by an inclined column member of a pyramidal truss core on left plate as a function of normalized imposed velocity V at three levels of overall strain and the result derived from an axially loaded column with three levels of initial imperfection. The insert on the left shows the dynamically loaded column (with $V/c_0\varepsilon_Y = 15$) while the insert on the left shows the quasistatically deformed column.

5 Summary

The dimensionless parameter $V/(\varepsilon_Y c_0)$ can be used to gauge whether coupled plastic wave propagation and lateral buckling occurs in columns whose ends experience a relative velocity V, and relatively strong dynamics occur when $V/(\varepsilon_Y c_0) > 5$. For relatively stocky columns, overall end-shortening corresponding to compressive strains of 20% or more can be achieved before appreciable bucking deformation occurs. The reaction force at the end of the column resisting the imposed motion is amplified by a factor of 2 or more above that for a quasistatically loaded column. Similarly, the energy dissipated in plastic deformation by the column at a given overall imposed strain is significantly increased due to the inertial stabilization of the column. The roles of the various geometric and material parameters are detailed in the paper for the case of constant velocity loading. These results provide insight into how columns can be expected to behave under other types of dynamic axial loading. The present paper reveals the importance of dynamic effects in the performance of truss cores of all-metal sandwich plates under high intensity dynamic loads.

Acknowledgments

This work has been supported in part by the ONR under Grant No. N00014-02-1-0700 and in part by the Division of Engineering and Applied Sciences, Harvard University. The authors acknowledge helpful discussions with N.A. Fleck and V. Deshpande.

References

[1] Xue, Z., and Hutchinson, J. W., 2004, "Preliminary assessment of sandwich plates subject to blast loads," Int. J. Mech. Sci., **45**, pp. 687–705.
[2] Johnson, W., and Reid, S. R., 1978, "Metallic energy dissipating systems," Appl. Mech. Rev., **31**, pp. 277–288.
[3] Abrahamson, G. R., and Goodier, J. N., 1966, "Dynamic flexural buckling of

rods within an axial plastic compression wave,'' J. Appl. Mech., **33**, pp. 241–247.
[4] Karagiozova, D., and Jones, N., 1996, ''Dynamic elastic-plastic buckling phenomena in a rod due to axial impact,'' Int. J. Impact Eng., **18**, pp. 919–947.
[5] Calladine, C. R., and English, R. W., 1984, ''Strain rate and inertia effects in the collapse of two types of energy-absorbing structures,'' Int. J. Mech. Sci., **26**, pp. 689–701.
[6] Anwen, W., and Wenying, T., 2003, ''Characteristic-value analysis for plastic dynamic buckling of columns under elastoplastic compression waves,'' Int. J. Non-Linear Mech., **38**, pp. 615–628.
[7] Lepik, Ulo, 2001, ''Dynamic buckling of elastic-plastic beams including effects of axial stress waves,'' Int. J. Impact Eng., **25**, pp. 537–552.
[8] Kenny, S., Pegg, N., and Taheri, F., 2002, ''Finite element investigations on the dynamic plastic buckling of a slender beam subject to axial impact,'' Int. J. Impact Eng., **27**, pp. 179–195.
[9] von Karman, T., and Duwez, P., 1950, ''The propagation of plastic deformation in solids,'' J. Appl. Phys., **21**, pp. 987–994.
[10] Taylor, G. I., 1958, *The Scientific Papers of G. I. Taylor*, Cambridge University Press, London, Vol. 1.
[11] ABAQUS/Explicit User's Manual, Version 6.2, Hibbit, Karlsson and Sorensen Inc., 2001.

PROOF COPY 005501AMJ